G.E. GRECHNEV, A.V. LOGOSHA, A.A. LYOGENKAYA, A.G. GRECHNEV, A.V. FEDORCHENKO

B. Verkin Institute for Low Temperature Physics and Engineering, Nat. Acad. of Sci. of Ukraine
(47, Lenin Ave., Kharkov 61103, Ukraine; e-mail: grechnev@ilt.kharkov.ua)

PACS 74.20.Pq, 74.62.Fj, 74.70.Dd, 74.70.Xa, 75.10.Lp

ELECTRONIC STRUCTURE AND PROPERTIES OF NOVEL LAYERED SUPERCONDUCTORS

The electronic energy structures and magnetic properties of layered superconductors RNi_2B_2C, RFe_4Al_8, and FeSe are systematically studied, by using the density functional theory (DFT). The calculations allowed us to reveal a number of features of the electronic structure, which can cause the manifestation of peculiar structural, magnetic and superconducting properties of these systems. It is demonstrated that the Fermi energy E_F is located close to the pronounced peaks of the electronic density of states (DOS). The main contribution to DOS at the Fermi level arises from 3d-electrons. The calculations of the pressure-dependent electronic structure and the magnetic susceptibility in the normal state indicate that the novel superconductors are very close to a magnetic instability with dominating spin paramagnetism. It is shown that experimental data on the pressure dependence of the superconducting transition temperature in FeSe correlate qualitatively with the calculated behavior of DOS at E_F as a function of the pressure.

K e y w o r d s: Electronic structure, magnetic superconductors, RNi$_2$B$_2$C, RFe$_4$Al$_8$, FeSe.

1. Introduction

The discovery of the superconductivity in transition metal borocarbides with the general formula RNi$_2$B$_2$C (R =Y, Ho, Er, Tm or Lu) and its coexistence with magnetism stimulated a considerable scientific interest in these systems [1]. Later, the superconductivity was also found in magnetic compounds YFe$_4$Al$_8$, LuFe$_4$Al$_8$, and ScFe$_4$Al$_8$ at temperatures lower than 6 K [2]. In 2008, the new class of iron-based layered superconductors was discovered. One of the representatives of this class is FeSe compound distinguished by the simplest crystal structure among iron-based superconductors and by the extremely large effect of a pressure on the superconducting transition temperature [3–5].

The characteristic feature of these layered compounds of 3d-metals is the well-established coexistence of magnetism and superconductivity. The relative structural simplicity of RNi$_2$B$_2$C, RFe$_4$Al$_8$, and FeSe is favourable for studying the effects of chemical substitution, high pressure, and uniaxial deformations on their physical properties. Such studies can reveal a mechanism of superconductivity in these systems, which contain magnetic 3d-metals.

The clarification of microscopic mechanisms, which determine electric and magnetic properties of metallic systems, assumes detailed experimental and theoretical studies of the electronic structure of a conduction band. A number of electronic structure calculations were carried out for nickel borocarbides [6, 7] and superconducting FeSe [8, 9] in recent years. However, the data on the electronic energy structure of these systems are still incomplete and inconsistent.

In very recent studies of magnetic superconductors with the angular resolved photoemission spectroscopy method (ARPES) [10], the presence of Van Hove singularities was established in the electronic structures in a small vicinity of the Fermi energy E_F. Moreover,

the technological progress in growing single-crystal samples provided an opportunity to study the fine structure of the electronic energy bands and the Fermi surface of nickel borocarbides by means of the de Haas–van Alphen effect [11, 12] and ARPES [13] and FeSe compound (ARPES, [14]). Thus, the detailed *ab initio* calculations of the electronic structure are necessary for the analysis of the spectral characteristics of these systems.

Here, we have calculated the electronic band structures and a number of thermodynamic characteristics of $R\mathrm{Ni_2B_2C}$, $R\mathrm{Fe_4Al_8}$, and FeSe compounds within the density functional theory (DFT) methods. The dependences of these characteristics on the volume and structural parameters were addressed to shed light on the corresponding high-pressure effects.

2. Details and Results of Electronic Structure Calculations

The calculations of electronic structures were carried out by using the modified relativistic LMTO method with a full potential (FP-LMTO, RSPt implementation [15, 16]) and the linearized augmented plane waves method with a full potential (FP-LAPW, Elk implementation [17]). The exchange and correlation potentials were treated within the local density approximation (LDA [18]) and the generalized gradient approximation (GGA [19]) of DFT. For the employed full potential FP-LMTO and FP-LAPW methods, any restrictions were not imposed on the charge densities or potentials of the studied systems, which is especially important for anisotropic layered structures of the investigated magnetic superconductors.

Electronic structure calculations for compounds were carried out for the sets of crystal lattice parameters close to experimental ones. Variations of the parameters of crystal lattices allow one to imitate the influence of an external pressure. In such a way, the volume dependence of the total energy of the electronic subsystem, $E(V)$, was calculated for the studied compounds. The theoretical values of equilibrium lattice parameters and bulk moduli B were determined from the calculated $E(V)$ dependences, by using the known Birch–Murnaghan equation of state (see Refs. [15, 16]).

To evaluate the paramagnetic susceptibility of compounds, the FP-LMTO calculations of field-induced spin and orbital (Van Vleck) magnetic moments were carried out with the approach described in Ref. [15] within the local spin density approximation (LSDA) of DFT. The relativistic effects, including spin-orbit coupling, were incorporated, and the effect of an external magnetic field $\mathbf{B}$ was taken into account self-consistently by means of the Zeeman term,

$$\mathcal{H}_Z = \mu_\mathrm{B}\mathbf{B}(2\hat{\mathbf{s}} + \hat{\mathbf{l}}). \tag{1}$$

Here, μ_B is the Bohr magneton, and $\hat{\mathbf{s}}$ and $\hat{\mathbf{l}}$ are the spin and orbital angular momentum operators, respectively. The field-induced spin and orbital magnetic moments provide the related contributions to the magnetic susceptibility, χ_spin and χ_orb.

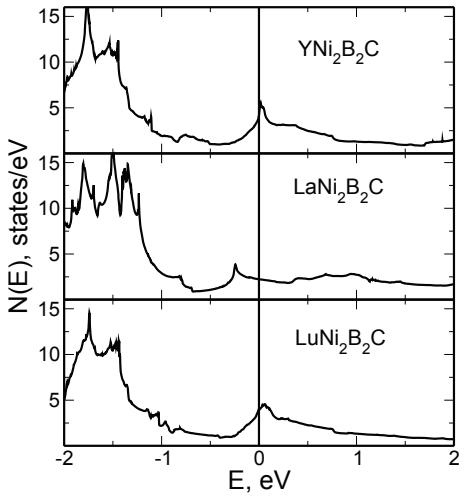

Fig. 1. Density of electronic states $N(E)$ of $\mathrm{YNi_2B_2C}$, $\mathrm{LaNi_2B_2C}$, and $\mathrm{LuNi_2B_2C}$ compounds. The Fermi level ($E = 0$) is marked by the vertical line

2.1. RNi_2B_2C

The crystal structure of nickel borocarbides (like $\mathrm{YNi_2B_2C}$, space group $I4/mmm$) is a body-centered tetragonal structure with alternating triple layers of B-Ni-B and Y-C planes. In this work, we carried out the DFT calculations of the band structures, densities of electronic states (DOS), and some thermodynamic characteristics of $\mathrm{YNi_2B_2C}$, $\mathrm{LaNi_2B_2C}$, and $\mathrm{LuNi_2B_2C}$ compounds. These compounds contain non-magnetic trivalent transition metals Y, La, and Lu, whose external electronic shells are similar to those of rare-earth elements R. For each compound, the calculations of the electronic structure were carried out for a number of lattice parameters, close to

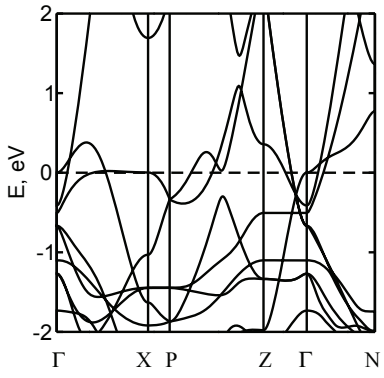

Fig. 2. Band structure of YNi_2B_2C along high symmetry lines of the Brillouin zone. The Fermi level ($E = 0$) is marked by the horizontal line

experimental ones (listed in Refs. [1, 20]). At the same time, the c/a ratio was fixed and corresponded to the experimental value for each RNi$_2$B$_2$C compound.

The calculated densities of electronic states $N(E)$ of these nickel borocarbides are similar, but differ in details and the positions of Fermi levels $E_{\rm F}$ (see Fig. 1). In Fig. 1, one can see the sharp peaks in $N(E)$ of YNi_2B_2C and $LuNi_2B_2C$ superconductors in a close proximity of the Fermi level, whereas the related peak in the non-superconducting $LaNi_2B_2C$ compound is situated much deeper below $E_{\rm F}$.

The calculated band structure of YNi_2B_2C compound is presented in Fig. 2, where one can see the presence of quasi-degenerate states near the Fermi level in a vicinity of the symmetry point Γ and at PZ line and the almost dispersion-free branch of $E(k)$ in the direction ΓX. The position of this branch corresponds to the sharp peak of DOS in a vicinity of $E_{\rm F}$ (Van Hove singularity in Fig. 1). The main contribution to $N(E_{\rm F})$ comes from the d-states of nickel layers.

The reliability of the present calculations of the electronic structure of nickel borocarbides is confirmed by a good description of the low-temperature quantum oscillation of magnetization – the de Haas–van Alphen effect (DHVA) – for YNi_2B_2C and $LuNi_2B_2C$ compounds [11, 12]. In particular, by comparison with the DHVA experimental data for YNi_2B_2C and $LuNi_2B_2C$, it is established that the low-frequency branches of DHVA oscillations found in [11, 12], $F_\alpha \simeq 500$ T, correspond to the Fermi surface sections in a vicinity of the symmetry point Γ (see $E(k)$ dependences in Fig. 2). It should be noted that, for a small shift of the Fermi level (less than 0.1 eV), which corresponds to the accuracy of the *ab initio* calculations of the Fermi energy position, the calculated sections of YNi_2B_2C and $LuNi_2B_2C$ Fermi surfaces appeared to be in agreement with F_α data from Refs. [11,12] within the experimental error. The ratio of experimental cyclotron masses to corresponding calculated ones, $m^c_{\rm exp}/m^c_{\rm theor} = (1 + \lambda)$, for the Fermi surface section F_α of YNi_2B_2C is within the limits of $1.5 \div 1.7$ for various directions of the magnetic field. This provides the reasonable value of the corresponding constant of many-body mass enhancement, $\lambda_\alpha \simeq 0.6$.

The calculated values of DOS at the Fermi level $N(E_{\rm F})$ for the nickel borocarbides are presented in Table 1 and can be compared with the available experimental data on the electronic specific heat coefficients $\gamma_{\rm exp}$ [21]. The differences between $\gamma_{\rm theor}$ and $\gamma_{\rm exp}$ are usually attributed to the renormalization of one-electron effective masses due to the electron-phonon interaction,

$$\gamma_{\rm exp} = (1 + \lambda)\gamma_{\rm theor}, \tag{2}$$

which gives a possibility to determine the corresponding renormalization parameter λ (see Table 1).

By using the theoretical and experimental data from Table 1, one can estimate the superconducting transition temperatures of the investigated nickel borocarbides with the use of the Macmillan formula [23]:

$$T_{\rm c} = \frac{\Theta_{\rm D}}{1.45} \exp\left[-\frac{1.04(1 + \lambda)}{\lambda - \mu^*(1 + 0.62\lambda)}\right], \tag{3}$$

where $\Theta_{\rm D}$ – Debye's temperature, λ – electron-phonon interaction constant, and μ^* – Morel–Anderson's Coulomb pseudopotential. The value of μ^* is taken to be 0.13, as accepted for transitional metals [23]. Thus, using the experimental values of Debye temperatures $\Theta_{\rm D}$ and estimated λ, we obtained T_c values, which are in a good agreement with experimental data for YNi_2B_2C and $LuNi_2B_2C$ (see Table 1). The difference of the estimated T_c with the experimental value for $LaNi_2B_2C$ can be caused either by errors in the evaluations of $\gamma_{\rm exp}$ and $N(E_{\rm F})$ or due to a large spin-fluctuation contribution $\lambda_{\rm sf}$ to the renormalization parameter λ in (2):

$$\lambda = \lambda_{\rm el-ph} + \lambda_{\rm sf}, \tag{4}$$

Table 1. **Thermodynamic properties of RNi$_2$B$_2$C borocarbides (R=Y, La, Lu). V – unit cell volume, $N(E_F)$ – DOS at the Fermi level, γ – electronic specific heat (Ref. [21]), Θ_D – Debye temperature (Ref. [21]), λ – electron-phonon mass enhancement, T_c – superconducting transition temperature (from [21, 22])**

Combination	V, Å^3	$N(E_F)$, states/eV·cell	γ(exp), mJ/mol·K^2	Θ_D, K	λ	T_c(exp), K	T_c(theor), K
YNi_2B_2C	65.9	4.30	18.2	490	0.8	15.6	15.3
$LaNi_2B_2C$	70.7	2.24	8.4	495	0.6	—	6.5
$LuNi_2B_2C$	63.8	4.07	19.5	360	1.0	16.6	17.8

which can explain a smaller contribution of λ_{el-ph}. Nevertheless, the results in Table 1 clearly testify in favor of the BCS-like electron-phonon mechanism of superconductivity in the nickel borocarbides, having $\lambda \approx 1$.

The FP-LMTO calculations of the field-induced spin and orbital (Van Vleck) magnetic moments were carried out for YNi_2B_2C, $LaNi_2B_2C$, and $LuNi_2B_2C$ compounds with inclusion of the Zeeman operator (1) in the external magnetic field $\mathbf{B} = 10$ T. For the tetragonal crystal structure, the corresponding contributions to the magnetic susceptibility, χ_{spin} and χ_{orb}, were calculated for the external field directed along the c axis. The values of magnetic susceptibility ($\chi_{theor} = \chi_{spin} + \chi_{orb}$) calculated for YNi_2B_2C, $LaNi_2B_2C$, and $LuNi_2B_2C$ are listed in Table 2 in comparison with the available experimental data.

In the general form, the total magnetic susceptibility can be decomposed in the following terms (see Ref. [15]):

$$\chi_{tot} = \chi_{spin} + \chi_{orb} + \chi_{dia} + \chi_L, \qquad (5)$$

which present, respectively, Pauli's spin susceptibility (χ_{spin}), Van Vleck orbital paramagnetism (χ_{orb}), Langevin diamagnetism of closed ion shells (χ_{dia}), and the orbital diamagnetism of conduction electrons (χ_L). It can be seen in Table 2 that the spin and orbital Van Vleck susceptibilities are the principal terms in Eq. (5). It is important that χ_{orb} gives a substantial contribution to the full paramagnetic susceptibility of borocarbides. The theoretical calculation of the Landau diamagnetism χ_L for the multiband dispersion law $E(k)$ represents a very difficult task [15]. However, a good fit of the experimental susceptibilities of YNi_2B_2C and $LuNi_2B_2C$ with the calculated paramagnetic contributions to χ (see Table 2) indicates that, in these superconducting systems, the diamagnetic contributions in (5) are insignificant.

Table 2. **Magnetic susceptibility of RNi$_2$B$_2$C ($R = Y$, La, Lu)**

Compound	χ_{spin}	χ_{orb}	χ_{theor}	χ_{exp}
	10^{-4} emu/mol			
YNi_2B_2C	1.35	0.87	2.22	2.0 [24]
$LaNi_2B_2C$	0.96	0.72	1.68	1.0 [24]
$LuNi_2B_2C$	1.29	0.73	2.02	1.9 [25]

2.2. RFe_4Al_8

Compounds RFe$_4$Al$_8$ possess the body-centered tetragonal crystal structure of the ThMn$_{12}$-type, which belongs to the $I4/mmm$ space symmetry group [26]. In case of non-magnetic trivalent transition metals (R = Sc, Y, Lu), the AFM ordering of iron moments was established in RFe$_4$Al$_8$ at low temperatures, though there are very inconsistent experimental data in the literature about a character of AFM ordering, ordering temperatures, and magnetic moments (see [2, 26–28] and references therein).

Virtually, no band structure calculations have been carried out to date for RFe$_4$Al$_8$. In work [27], the main attention was paid to calculations of the iron magnetic moments in the magnetically ordered phases of YFe_4Al_8. In the present work, the DFT electronic calculations are carried out for YFe_4Al_8, $ScFe_4Al_8$, and $LuFe_4Al_8$ compounds in the paramagnetic, ferromagnetic (FM), and antiferromagnetic (AFM) phases.

The calculated DOS of the paramagnetic phase of $LuFe_4Al_8$ is presented in Fig. 3. The densities

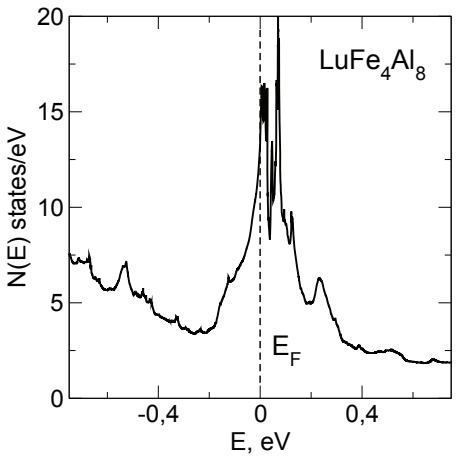

Fig. 3. Density of electronic states $N(E)$ of $LuFe_4Al_8$ in the paramagnetic phase. The Fermi level ($E = 0$) is marked by the vertical line

of states $N(E)$ for the isoelectronic $ScFe_4Al_8$ and YFe_4Al_8 compounds are very similar, and they differ in small details only. The calculated densities of states at the Fermi level are listed in Table 3, and the dominating contributions to $N(E_F)$ come from the d-states of iron. As is seen from Fig. 3, the Fermi level for the PM phase of $LuFe_4Al_8$ is located at the steep slope of the density of states, where $N(E)$ quickly grows with the energy in the immediate proximity (∼0.01 eV) to the sharp peak of DOS.

The peak of $N(E)$ in Fig. 3 is split at the AFM ordering for spin-up and spin-down states, and this provides the formation of the magnetic moments on the iron atom. As is seen from Table 3, it is accompanied by a noticeable decrease in $N(E_F)$ for the ferromagnetic and antiferromagnetic phases of RFe_4Al_8. The

Table 3. **Densities of electronic states at the Fermi level and the magnetic moments of iron atoms for RFe_4Al_8 compounds (R = Sc, Y, Lu) in the paramagnetic (PM), ferromagnetic (FM) and antiferromagnetic (AFM) phases**

Combination	$N(E_F)$ states/(eV·cell)			M μ_B	
	PM	FM	AFM	FM	AFM
$ScFe_4Al_8$	25.2	10.5	14.5	1.20	1.17
YFe_4Al_8	26.5	8.4	14.7	1.27	1.25
$LuFe_4Al_8$	27.0	11.5	14.3	1.24	1.22

distinction between the magnetic moments on a Fe atom for the FM and AFM phases appeared insignificant in the case of $LuFe_4Al_8$ and more noticeable in $ScFe_4Al_8$. For all three investigated RFe_4Al_8 compounds, the minimum of the total energy is found for the AFM ordering of the Fe moments in the basal plane along the [100] type directions. The calculated values of magnetic moments from Table 3 are qualitatively consistent with the experiments of Ref. [28] for $LuFe_4Al_8$ ($\simeq 1.3\mu_B$) and the results of calculations in [27] for YFe_4Al_8 ($\simeq 1.25\mu_B$).

The calculated value of DOS at the Fermi level for the AFM phase of $LuFe_4Al_8$, $N(E_F) = 14.3$ states/(eV· cell), can be compared with experimental data on the electronic specific heat coefficient in this compound, $\gamma_{exp} = 70$ mJ/mol · K^2 [2]. According to (2), the corresponding renormalization parameter for effective masses is about $\lambda \simeq 1$, which is qualitatively consistent with the observation of superconductivity in $LuFe_4Al_8$ [2]. It is necessary to consider, however, a contribution of the spin-fluctuation term in (4), which can be rather large for systems with high values of $N(E_F)$, to λ [15]. Therefore, the question remains open: Can spin-fluctuations affect superconductivity in RFe_4Al_8 compounds and, if so, how?

2.3. FeSe

The calculations of the electronic structure of FeSe were performed for the tetragonal $P4/nmm$ structure and for the orthorhombic $Cmma$ structure, which correspond to the non-magnetic superconducting phase. The crystal lattice parameters of FeSe were taken according to data of Refs. [3,4,29,30]. The calculated density of electronic states of the tetragonal FeSe is presented in Fig. 4, where the dominating contribution to $N(E_F)$ comes from the 3d-states of iron.

As is seen in Fig. 4, the Fermi level is located in a close proximity (∼0.1 eV) to the sharp peak of the density of electronic states. A similar feature of $N(E)$ near E_F appears also in the orthorhombic phase of FeSe. It should be noted that fine details of the electronic spectrum, in particular, positions of the critical points of $E(k)$ relatively to E_F, can be reliably determined by the *ab initio* calculations within DFT with an accuracy no more than 0.1 eV.

According to the results of calculations of the electronic structure and the magnetic susceptibility in the normal state in an external magnetic field, FeSe com-

pound is very close to a magnetic instability with the dominating exchange-enhanced spin paramagnetism $\chi_{\rm spin}$. Within the Stoner model, the exchange-enhanced Pauli spin contribution to the magnetic susceptibility can be presented as $\chi_{\rm ston} = S\mu_{\rm B}^2 N(E_{\rm F})$, where S – the Stoner factor, $N(E_{\rm F})$ – the density of states at the Fermi level, $\mu_{\rm B}$ – the Bohr magneton. The calculated value of DOS at the Fermi level for FeSe amounts to $N(E_{\rm F}) \simeq 1$ states/(eV·cell), allowing a small uncertainty in the determination of lattice parameters. Using the experimental value of susceptibility of FeSe at low temperatures, $\chi \simeq 1.6 \times 10^{-4}$ emu/mol [31], we obtained the Stoner factor $S \simeq 5$.

The calculated $N(E_{\rm F})$ can be compared with experimental data on the electronic specific heat coefficient in FeSe, $\gamma_{\rm exp} = 5.73$ mJ/mol·K^2 [32]. According to (2), the corresponding parameter of renormalization of the effective masses amounts to $\lambda \simeq 1.4$. Assuming the validity of formalism (3) for the superconducting transition in FeSe at 8 K and using the experimental value $\Theta_{\rm D} = 210$ K from [32], it is possible to estimate the corresponding electron-phonon interaction parameter, $\lambda_{\rm el-ph} \simeq 0.9$. However, it is necessary to consider also the spin-fluctuation term, according to (4), which gives $\lambda_{\rm sf} \simeq 0.5$.

The experimentally observed large effects of a pressure on the superconducting transition temperature [3, 4] and on the magnetic susceptibility [31] gave evidence of substantial changes in the electronic structure of FeSe under pressure. In order to clarify a nature of these changes, the geometry optimization was performed for the tetragonal $P4/nmm$ structure of FeSe within the GGA approach [19] and Elk program [17]. In a such way, the pressure dependences of the crystal lattice parameters were calculated. In particular, a growth of the relative height Z of selenium atoms over the iron atoms plane under applied pressure was established. These results are in a qualitative agreement with experimental data of Refs. [29, 30].

With the use of the established dependences of lattice parameters of FeSe under pressure, we have calculated the corresponding behavior of DOS at the Fermi level, $N(E_{\rm F}, P)$, which is presented in Fig. 5. It should be noted that the value of $N(E_{\rm F}, P = 0)$ calculated within the GGA approach is by ∼1.5 times larger than the corresponding value in Fig. 4, which was calculated in the LDA approach [18]. For the

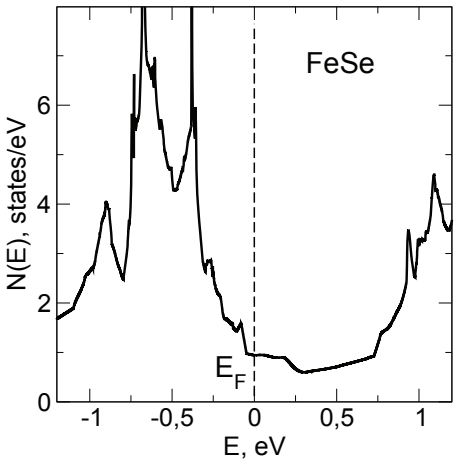

Fig. 4. Density of electronic states $N(E)$ of FeSe. The Fermi level ($E = 0$) is marked by the vertical line

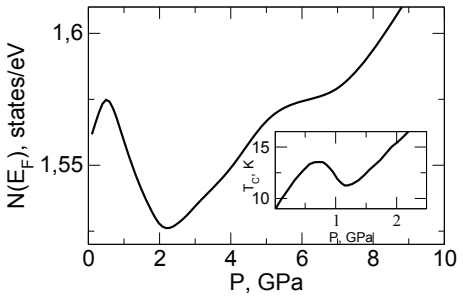

Fig. 5. Pressure dependence of the density of electronic states of FeSe at the Fermi level, $N(E_{\rm F})$. The inset shows the pressure dependence of the superconducting transition temperature for FeSe taken from Ref. [5]

small pressures ($0 \div 0.3$ GPa, see Fig. 5), the calculated derivative $\mathrm{d}\ln N(E_{\rm F})/\mathrm{d}P \simeq 2.7 \times 10^{-2}$ GPa^{-1} is in a qualitative agreement with the experimental value of the derivative of the magnetic susceptibility with respect to the pressure at low temperatures, $\mathrm{d}\ln\chi/\mathrm{d}P \simeq 10 \times 10^{-2}\,\mathrm{GPa}^{-1}$ ($0 < p < 0.2$ GPa, [31]), with regard for the Stoner factor of exchange enhancement ($S \simeq 5$). Basically, the experimentally observed large positive pressure effect on χ in FeSe at low temperatures [31] is caused by an increase of the internal structural parameter Z under pressure.

It should be noted that the calculated dependence of $N(E_{\rm F}, P)$ in Fig. 5 correlates with the specific non-monotonic behavior of the superconducting transition temperature in the FeSe compound in a wide range of pressures [5] (see inset in Fig. 5). Such compliance can testify either in favor of the BCS mechanism of su-

perconductivity, or an alternative mechanism, which could involve, in a similar fashion, the density of electronic states at the Fermi level.

3. Conclusions

The calculations of the densities of electronic states of $R\mathrm{Ni_2B_2C}$, $R\mathrm{Fe_4Al_8}$, and FeSe compounds indicate that the Fermi energy in these systems is located in a vicinity of the pronounced peaks in $N(E)$. This confirms the recent ARPES observations that the proximity of Van Hove spectral features to the Fermi level can be considered as a key component for a realization of the superconductivity in transition metal compounds [10]. Though the main contribution to DOS for all three systems in a vicinity of E_F comes from the quasi-two-dimensional layers of 3*d*-metal atoms, nickel and iron, the $N(E)$ dependences appear to be notably different. The Fermi level in $R\mathrm{Fe_4Al_8}$ is located just at the peak of $N(E)$ and in the area of high values of DOS. As for $R\mathrm{Ni_2B_2C}$ and FeSe compounds, the Fermi level is actually in the "pseudo-gap" area of electronic spectra with rather low values of $N(E_\mathrm{F})$.

The results of calculations of the electronic structure allow us to analyze the experimental data on the electronic specific heat coefficient (in $R\mathrm{Ni_2B_2C}$, $\mathrm{LuFe_4Al_8}$, FeSe) and the cyclotron masses (DHVA effect in $\mathrm{YNi_2B_2C}$ and $\mathrm{LuNi_2B_2C}$). The estimated renormalization parameters of the effective mass of conduction electrons indicate a possibility to realize the electron-phonon mechanism of superconductivity in these systems with $\lambda_{\mathrm{el-ph}} \simeq 1$. Along with this, the estimates indicate a noticeable contribution of the electron-paramagnon (spin-fluctuation) interactions to λ, which complies with a proximity of $R\mathrm{Ni_2B_2C}$, $R\mathrm{Fe_4Al_8}$ and FeSe to the magnetic ordering.

It is shown that the available experimental data on the strong pressure dependence of the magnetic susceptibility and the superconducting transition temperature in FeSe are caused by an increase in the density of electronic states at the Fermi level under pressure. The experimentally established nonmonotonic dependence of the superconducting transition temperature on the pressure in FeSe qualitatively correlates with the calculated behavior of DOS at the Fermi level in a wide range of pressures (Fig. 5).

This work was supported by the Russian-Ukrainian RFBR-NASU project 01-02-12.

1. K.-H. Müller, M. Schneider, G. Fuchs, and S.-L. Drechsler, in: *Handbook on the Physics and Chemistry of Rare Earths*, edited by K.A. Gscheidner, jr., J.-C.G. Bünzli, and V.K. Pecharsky (Elsevier, Amsterdam, 2008), p. 175.
2. V.M. Dmitriev, N.N. Prentslau, I.V. Zolochevskii, L.A. Ishchenko, A.V. Terekhov, B.Ya. Kotur, W. Suski, and E. Talik, Low Temp. Phys. **29**, 901 (2003).
3. Y. Mizuguchi and Y. Takano, J. Phys. Soc. Jpn. **79**, 102001 (2010).
4. J. Wen, G. Xu, G. Gu, J.M. Tranquada, and R.J. Birgeneau, Rep. Progr. Phys. **74**, 124503 (2011).
5. M. Bendele, A. Ichsanow, Yu. Pashkevich, L. Keller, Th. Strassle, A. Gusev, E. Pomjakushina, K. Conder, R. Khasanov, and H. Keller, Phys. Rev. B **85**, 064517 (2012).
6. M. Divis, K. Schwarz, P. Blaha, G. Hilscher, H. Michor, and S. Khmelevskyi, Phys. Rev. B **62**, 6774 (2000).
7. A.O. Shorikov, V.I. Anisimov, and M. Sigrist, J. Phys.: Condens. Matter **18**, 5973 (2006).
8. A. Subedi, L. Zhang, D.J. Singh, and M.H. Du, Phys. Rev. B **78**, 134514 (2008).
9. K.-W. Lee, V. Pardo, and W.E. Pickett, Phys. Rev. B **78**, 174502 (2008).
10. A.A. Kordyuk, Low Temp. Phys. **38**, 901 (2012).
11. G. Goll, M. Heinecke, A.G.M. Jansen, W. Joss, L. Nguyen, E. Steep, K. Winzer, and P. Wyder, Phys. Rev. B **53**, R8871 (1996).
12. B. Bergk and J. Wosnitza, Low Temp. Phys. **35**, 687 (2009).
13. T. Baba, T. Yokoya, S. Tsuda, T. Watanabe, M. Nohara, H. Takagi, T. Oguchi, and S. Shin, Phys. Rev. B **81**, 180509(R) (2010).
14. J. Maletz, V.B. Zabolotnyy, D.V. Evtushinsky, S. Thirupathaiah, A.U.B. Wolter, L. Harnagea, A.N. Yaresko, A.N. Vasiliev, D.A. Chareev, E.D.L. Rienks, B. Büchner, and S.V. Borisenko, arXiv:1307.1280 [cond-mat.supr-con] (2013).
15. G.E. Grechnev, Low Temp. Phys. **35**, 638 (2009).
16. J.M. Wills, M. Alouani, P. Andersson, A. Delin, O. Eriksson, A. Grechnev, *Full-Potential Electronic Structure Method. Energy and Force Calculations with Density Functional and Dynamical Mean Field Theory* (Springer, Berlin, 2010).
17. http://elk.sourceforge.net/
18. U. von Barth and L. Hedin, J. Phys. C: Solid State Phys. **5**, 1629 (1972).
19. J.P. Perdew, K. Burke, and M. Ernzerhof, Phys. Rev. Lett. **77**, 3865 (1996).
20. J.W. Lynn, S. Skanthakumar, Q. Huang, S.K. Sinha, Z. Hossain, L.C. Gupta, R. Nagarajan, and C. Godart, Phys. Rev. B **55**, 6584 (1997).
21. H. Michor, T. Holubar, C. Dusek, and G. Hilsher, Phys. Rev. B **52**, 16165 (1995).
22. D.R. Sanchez, S.L. Bud'ko, and E.M. Baggio-Saitovitch, J. Phys.: Condens. Matter **12**, 9941 (2000).
23. W.L. McMillan, Phys. Rev. **167**, 331 (1968).

24. I.R. Fisher, J.R. Cooper, and R.J. Cava, Phys. Rev. B **52**, 15086 (1995).
25. C.C. Lai, M.S. Lin, Y.B. You, and H.C. Ku, Phys. Rev. B **51**, 420 (1995).
26. H. Misiorek, J. Stepien-Damm, W. Suski, E. Talik, B.Y. Kotur, and V.M. Dmitriev, J. Alloys Comp. **363**, 78 (2004).
27. C. Cardoso, T. Gasche, and M. Godinho, J. Phys.: Condens. Matter **18**, 8817 (2006).
28. J.A. Paixao, M. Ramos Silva, J.C. Waerenborgh, A.P. Goncalves, G.H. Lander, P.J. Brown, M. Godinho, and P. Burlet, Phys. Rev. B **63**, 054410 (2001).
29. J. N. Millican, D. Phelan, E.L. Thomas, J.B. Leao, and E. Carpenter, Solid State Commun. **149**, 707 (2009).
30. R.S. Kumar, Y. Zhang, S. Sinogeikin, Y. Xiao, S. Kumar, P. Chow, A.L. Cornelius, and C. Chen, J. Phys. Chem. B **114**, 12597 (2010).
31. G.E. Grechnev, A.S. Panfilov, V.A. Desnenko, A.V. Fedorchenko, S.L. Gnatchenko, D.A. Chareev, O.S. Volkova, and A.N. Vasiliev, J. Phys.: Condens. Matter **25**, 046004 (2013).
32. J.Y. Lin, Y.S. Hsieh, D.A. Chareev, A.N. Vasiliev, Y. Parsons, and H.D. Yang, Phys. Rev. B **84**, 220507(R) (2011).

Received 23.09.13

Г.Є. Гречнєв, О.В. Логоша,
А.О. Легенька, О.Г. Гречнев, О.В. Федорченко

ЕЛЕКТРОННА СТРУКТУРА І ВЛАСТИВОСТІ НОВІТНІХ ШАРУВАТИХ НАДПРОВІДНИКІВ

Р е з ю м е

На основі теорії функціонала густини (DFT) проведено систематичне вивчення електронної енергетичної структури і магнітних властивостей шаруватих надпровідників $R\mathrm{Ni_2B_2C}$, $R\mathrm{Fe_4Al_8}$ і FeSe. Обчислення дозволили виявити ряд специфічних особливостей електронної структури, що можуть відповідати за незвичайні структурні, магнітні та надпровідні властивості цих систем. Продемонстровано, що енергія Фермі розташована в околі піків густини електронних станів (DOS). Головний внесок в DOS на рівні Фермі дають $3d$-електрони. Обчислення ефектів тиску на електронну структуру і магнітну сприйнятливість у нормальному стані вказують, що в цих новітніх надпровідниках домінує спіновий парамагнетизм, і вони близькі до магнітної нестабільності. Показано, що експериментальні дані по залежності температури надпровідного переходу в FeSe від тиску якісно корелюють з розрахованою поведінкою DOS на рівні Фермі під тиском.